



CHORUS

This is the accepted manuscript made available via CHORUS. The article has been published as:

Oxidation of Pt(111) under Near-Ambient Conditions

D. J. Miller, H. Öberg, S. Kaya, H. Sanchez Casalongue, D. Friebel, T. Anniyev, H. Ogasawara, H. Bluhm, L. G. M. Pettersson, and A. Nilsson

Phys. Rev. Lett. **107**, 195502 — Published 4 November 2011

DOI: [10.1103/PhysRevLett.107.195502](https://doi.org/10.1103/PhysRevLett.107.195502)

Oxidation of Pt(111) under near-ambient conditions

D. J. Miller^{1,2}, H. Öberg³, S. Kaya^{1,2}, H. Sanchez Casalongue², D. Friebe^{1,2}, T. Anniyev^{1,2}, H. Ogasawara², H. Bluhm^{4,5}, L. G. M. Pettersson³ and A. Nilsson^{1,2,3,*}

¹*Stanford Institute for Materials and Energy Sciences, SLAC National Accelerator Laboratory, 2575 Sand Hill Rd, Menlo Park, CA 94025 USA*

²*Stanford Synchrotron Radiation Lightsource, SLAC National Accelerator Laboratory, 2575 Sand Hill Rd, Menlo Park, CA 94025, USA*

³*Department of Physics, AlbaNova University Center, Stockholm University, S-106 91 Stockholm, Sweden*

⁴*Advanced Light Source, Lawrence Berkeley National Lab, Berkeley, CA 94720, USA*

⁵*Chemical Science Division, Lawrence Berkeley National Lab, Berkeley, CA 94720, USA*

PACS numbers: 81.65.Mg, 68.43.Fg, 68.43.Bc, 82.65.+r

Abstract:

The oxidation of Pt(111) at near-ambient O₂ pressures has been followed *in situ* using x-ray photoelectron spectroscopy (XPS) and *ex situ* using x-ray absorption spectroscopy (XAS). Polarization dependent XAS signatures at the O *K*-edge reveal significant temperature- and pressure-dependent changes of the Pt–O interaction. Oxide growth commences via a PtO-like surface oxide that coexists with chemisorbed oxygen, while an ultrathin α -PtO₂ trilayer is identified as the precursor to bulk oxidation. These results have important implications for understanding the chemical state of Pt in catalysis.

26 Surface oxides with markedly different activities than the metallic surface can form
27 under the O₂-rich conditions employed in many Pt-based industrial processes [1],
28 including the electrochemical oxygen reduction reaction (ORR) [2], CO oxidation [3–5]
29 and the Ostwald process [6]. However, surface-sensitive techniques that can distinguish
30 different oxidation states, e.g., electron-based spectroscopies, are mostly incompatible
31 with the elevated O₂ pressures ($> 10^{-5}$ Torr) required to oxidize Pt. Consequently, even
32 though (111)-oriented facets are the most abundant close-packed surfaces on the Pt
33 nanoparticles [7] typically employed in industrial catalysis, oxide growth on Pt(111)
34 remains poorly understood.

35 Exposing Pt(111) to O₂ under ultrahigh vacuum (UHV) conditions yields
36 chemisorbed $p(2 \times 2)$ -O domains with an oxygen coverage, θ , at saturation of
37 0.25 ML [8,9]. However, oxygen phases with $\theta > 0.25$ ML can be prepared in UHV
38 either by using reactive oxygen species, e.g., NO₂ [10–12] and atomic oxygen
39 beams [13,14], or by irradiating saturated O₂ adlayers, e.g., with x-rays [15]. In
40 particular, NO₂ yields a network of linear protrusions that was ascribed to a surface-oxide
41 phase with square-planar Pt–O coordination similar to that of bulk PtO [10].

42 The first *in situ* studies of Pt(111) under high O₂ partial pressures employed surface
43 x-ray diffraction (SXRD) [16]. At near-atmospheric O₂ pressures (>380 Torr) and above
44 520 K the formation of O–Pt–O trilayers similar to those found in α -PtO₂ is
45 observed [16]. However, the precursors to the trilayer oxide have not been characterized;
46 in particular, it is unknown whether the PtO-like surface oxide identified in UHV could
47 also form at elevated O₂ pressures, i.e., under conditions approaching those found in
48 heterogeneous catalysis.

49 Using a photoemission system that can operate at near-ambient pressures ($P <$
50 5 Torr) [17], we have followed the oxidation of Pt(111) by O₂ by means of x-ray
51 absorption (XAS) and x-ray photoelectron (XPS) spectroscopies. With the aid of density
52 functional theory (DFT) simulations, we demonstrate that oxide growth involves phase
53 transitions from chemisorbed O to two different surface oxides whose structures resemble
54 PtO in the initial stages of oxidation and α -PtO₂ at the onset of bulk oxidation.

55 The experiments were performed at beamline 11.0.2 of the Advanced Light Source
56 (ALS) using the ambient-pressure XPS endstation [17]. Oxygen layers were prepared by
57 dosing a Pt(111) crystal (cleaned using standard procedures [8]) with up to 5 Torr O₂.
58 XPS was performed *in situ*, while Auger-yield XAS was measured after evacuating O₂,
59 i.e., under UHV conditions; XPS confirmed that the oxygen layers were stable during
60 spectral acquisition. DFT calculations [18] using the PBE exchange-correlation
61 functional [19] were performed with the GPAW program [20,21], which is a real-space-
62 grid-based all-electron DFT code implemented in the projector augmented wave [22]
63 (PAW) formalism. XAS spectra were calculated [23] using the half-core-hole transition
64 potential approach [24], as implemented in GPAW [25].

65 XPS spectra for O/Pt(111) with coverages up to 2.1 ML are shown in Fig. 1. Surface
66 and bulk Pt atoms of adsorbate-free Pt(111) give rise to Pt 4f_{7/2} components at 70.5 and
67 70.9 eV, respectively [8]. The formation of *p*(2 × 2)-O domains at 1 × 10⁻⁵ Torr O₂ and
68 300 K yields an additional “chemisorbed” Pt 4f_{7/2} component at 71.1 eV, an asymmetric
69 O 1s structure at 529.7 eV [8,26], and a single XAS peak close to threshold (~529.9 eV)
70 for both in-plane and out-of-plane polarizations [Fig. 2(a)]. As found in Ref. [8], the out-
71 of-plane spectrum is slightly broader and more intense; otherwise, pronounced
72 polarization dependence is not observed. GPAW simulations [Fig. 2(b)] reproduce all
73 salient features of the observed spectra, thus validating the adopted theoretical approach.

74 With *P*(O₂) fixed at 0.5 Torr, the coverage rises steadily from 0.4 ML at *T* = 300 K
75 until saturation (1.1 ML) is attained at ~620 K. Other than the disappearance of the
76 surface peak, below 0.6 ML the only discernible change in Pt 4f XPS is a slight
77 broadening of the chemisorbed component toward high binding energy (B.E.). The
78 corresponding XAS spectra are qualitatively similar in all respects to those obtained at
79 0.25 ML and, as in previous experimental [10] and theoretical studies [27,28], are best
80 reproduced by chemisorbed structure models in which the O adatoms occupy fcc sites,
81 i.e., our results support the growth of *p*(2 × 1)-O domains.

82 An additional Pt 4f feature between 71.6 and 71.7 eV (“4O”) grows in above 420 K
83 when *P*(O₂) = 0.5 Torr (0.6 < *θ* < 1.1 ML). This is accompanied by a ~ -0.2 eV shift of
84 the O 1s XPS peak, which, while smaller than the experimental resolution (~0.3 eV), is

85 matched by a comparable shift of the O *K*-edge absorption threshold, as expected for a
86 system with metallic screening of the core-ionized $O1s^{-1}$ final state. The concomitant
87 observation of strongly polarization-dependent XAS signatures confirms the growth of a
88 chemically distinct new oxygen phase. In particular, we observe an additional high-
89 energy XAS feature that is significantly more pronounced and located $\sim +0.7$ eV
90 (531.6 eV) higher in energy in the in-plane spectrum.

91 To address whether the “4O” phase could coexist with chemisorbed O, an oxygen
92 layer generated at 0.5 Torr and 570 K ($\theta = 0.8$ ML) was exposed to 2×10^{-8} Torr H_2 [Fig.
93 3(a)]. Removing up to 0.5 ML of this layer suppressed the near-threshold peak of the in-
94 plane XAS spectrum without significantly affecting the high-energy feature; accordingly,
95 the “4O” Pt *4f* peak attenuates more rapidly than the chemisorbed component [Figs. 3(a)
96 and 3(c)]. We note, however, that the “4O” layers could be removed completely by
97 longer H_2 exposures (> 4 L, 1 L = 1×10^{-6} Torr s). Since the high-energy feature exhibits
98 no energy shift and the XAS spectra of the 0.3 ML H_2 -treated oxygen layer and a
99 saturated “4O” layer (1.1 ML) are in good agreement, H_2 -induced structural
100 rearrangements cannot explain the attenuation of the near-threshold peak. The high-
101 energy feature is therefore associated exclusively with the “4O” phase, whereas the near-
102 threshold peak can contain an additional chemisorbed contribution. We moreover assign
103 the double-peaked signature of the 0.30 ML H_2 -treated layer [Fig. 3(a)] to a nearly pure
104 “4O” phase.

105 The strong polarization dependence of the “4O” XAS spectrum indicates a highly
106 anisotropic ligand field of the surface Pt atoms: simulations of high-coverage (i.e., $\theta >$
107 0.5 ML) all-fcc chemisorbed structures and high-symmetry subsurface configurations
108 (e.g., the tetrahedral hollow located below the on-surface hcp site) fail to reproduce the
109 observed spectra. The “4O” phase exhibits O *1s* and Pt *4f* core-level shifts [$\Delta_O \sim -0.2$ eV,
110 $\Delta_{Pt} \sim +0.7-0.8$ eV, measured with respect to *p*(2×2)-O (529.7 eV) and bulk Pt (70.9 eV),
111 respectively] highly comparable to those reported for 1D oxide chains with square-planar
112 Pt–O coordination that form at the step edges of Pt(533) [6] ($\Delta_{Pt} \sim +0.55-0.65$ eV) and
113 Pt(332) [4] ($\Delta_O \sim -0.2$ eV, $\Delta_{Pt} = +0.45 \pm 0.07$ eV), indicating that the coordination
114 environment within the “4O” phase could be similar. Accordingly, the “4O” XAS

115 signature is qualitatively reproduced using the 1 ML surface-oxide model structure
116 depicted in Fig. 2(b), which comprises extended oxide chains with Pt–O bonds oriented
117 almost parallel ($\sim 15^\circ$) to the (111) plane. This structure, proposed by Hawkins *et al.* [28],
118 is generated by occupying selected hcp sites between the close-packed oxygen rows of
119 the $p(2 \times 1)$ -O phase [28] and represents the most stable 1 ML configuration identified by
120 those authors using a (2×2) supercell.

121 However, the 1 ML structure can be relaxed further by using larger supercells.
122 Indeed, a single oxide stripe adsorbed on a $(2\sqrt{3} \times 4)$ supercell of Pt(111) yields improved
123 agreement with the observed “4O” spectrum [Fig. 2(b)]: the separation between the near-
124 threshold and high-energy in-plane features (2.2 eV) better matches experiment (2.1 eV),
125 while the high-energy shoulder observed in the out-of-plane direction is now reproduced.
126 Additional simulations (not shown) indicate that the reduced peak separation arises from
127 the longer Pt–O bonds of the isolated stripe ($d = 1.95, 2.06 \text{ \AA}$ vs. $1.93, 1.96 \text{ \AA}$ in the
128 original structure): whereas the stripe can adopt a local configuration resembling bulk
129 PtO ($d = 2.04 \text{ \AA}$), bond lengthening in the 1 ML structure incurs a large energy penalty.
130 The high-energy shoulder in the out-of-plane spectrum arises from the increased tilt of
131 the isolated stripe with respect to the (111) plane ($\sim 29^\circ$ vs. $\sim 15^\circ$), which enhances the
132 spectral weight of O $2p$ hybrid orbitals associated with Pt–O σ^* bonds. Although the
133 absence of a superstructure in LEED prevents more detailed structural conclusions, our
134 simulations clearly identify the “4O” phase as a surface oxide comprising square-planar
135 PtO₄ units.

136 Drastic changes in both O $1s$ and Pt $4f$ XPS are observed upon exposure to ~ 5 Torr
137 O₂ above 720 K ($\theta > 1.1$ ML): the O $1s$ peak broadens and shifts to higher B.E., while the
138 Pt $4f$ spectrum exhibits—in addition to the bulk peak—two broad, similarly intense
139 features at 72.1 and 73.5 eV. The latter component was also observed after exposing
140 Pt(111) to atomic O [13,14] and *ex situ* following reaction with 750 Torr O₂ at
141 900 K [29]; given the 74.1 eV B.E. of bulk α -PtO₂, it is assigned to Pt atoms with six O
142 nearest neighbors. As demonstrated below, these highly oxidized Pt atoms reside within
143 α -PtO₂(0001) trilayers. Assuming that the surface is uniformly covered by these trilayers,
144 a simple argument based on the mismatch between the in-plane lattice constants of α -

145 PtO₂ (3.10 Å) and Pt(111) (2.77 Å) leads to an estimate of ~1.3 trilayers when $\theta =$
146 2.1 ML. However, only a weak (1 × 1) structure is observed in LEED, suggesting that the
147 PtO₂-like oxide most likely exists as small domains comprising one or two trilayers.

148 The Pt 4*f* feature at lower B.E. (72.1 eV) is ascribed to Pt atoms at the interface
149 between trilayer and metallic substrate; the smaller Δ_{Pt} arises from both reduced O
150 coordination and more effective metallic screening. The broadened O 1*s* peak indicates
151 that at least two chemically distinct oxygen species are present. We identify two
152 components at 529.7 and 530.1 eV, which on the basis of screening arguments and the
153 binding energies of chemisorbed O (529.7 eV [8]) and bulk α -PtO₂ (530.2 eV [29]) are
154 assigned to O atoms in the lower and upper layers of the trilayer, respectively. While we
155 are unable to identify XAS features associated with adsorbed OH or H₂O [30], additional
156 measurements, e.g., using vibrational spectroscopy, are required to completely exclude
157 that termination of the oxide surface by such species contributes to the broadening of the
158 O 1*s* XPS feature.

159 PtO₂-trilayer formation coincides with drastic changes in the polarization dependence
160 of XAS, which indicates large rearrangements of the coordination environment of the
161 surface Pt atoms. Both in-plane and out-of-plane spectra now exhibit a single broad peak
162 centered at 531.5 and 530.8 eV, respectively, which is associated with transitions to
163 unoccupied O 2*p*-Pt 5*d* hybrid states. Partial removal of the trilayer oxide using 2×10^{-8}
164 Torr H₂ did not induce discernible changes in XAS [Fig. 3(b)]; accordingly, the two
165 oxide-derived Pt 4*f* XPS components attenuate at comparable rates upon H₂ exposure
166 [Fig. 3(d)]. Similar behavior was observed for the trilayer oxide that forms on
167 Rh(111) [31] and clearly indicates that a single phase of oxidic Pt is present beyond
168 1.1 ML. XAS simulations of a single trilayer on Pt(111) are shown in Fig. 2(b). The
169 simulations predict a single peak near-threshold that is shifted to higher energy (~
170 +0.4 eV) in the in-plane spectrum, which agrees well with the observed +0.6 eV shift. We
171 therefore propose that the Pt coordination environment within the surface oxide generated
172 at 2.1 ML resembles the octahedral ligand field of bulk α -PtO₂.

173 In summary, beyond a critical chemisorbed coverage of ~0.50 ML the oxidation of
174 Pt(111) proceeds via a PtO-like surface-oxide phase, followed by PtO₂-like trilayers that

175 could nucleate at steps or defects [32]. A comparison with oxide growth on other *4d* and
176 *5d* Pt-group metals is instructive. Pd(111) also forms a surface oxide, Pd₅O₄, that coexists
177 with chemisorbed O [33], but at oxygen chemical potentials much lower than those
178 required to generate the PtO-like phase. This suggests that there is a greater kinetic
179 hindrance to Pt oxidation, which could be associated with the larger cohesion energy of
180 Pt (−5.84 eV) compared to Pd (−3.89 eV); that PtO-like oxide chains form on the more
181 open (2 × 1)-Pt(110) surface already at 355 K and ~0.01 Torr supports this
182 interpretation [34,35]. Interestingly, whereas the ultrathin trilayer oxide identified on
183 Pt(111) is preceded by a PtO-like surface oxide, analogous oxidic precursors to the
184 trilayer phases that form on Rh(111) [31,36] and Ir(111) [37] have not been found; the
185 elevated temperatures required to initiate bulk-oxide growth on all three surfaces suggest,
186 however, that the trilayer phase passivates the surface against further oxidation.

187 The role of the Pt surface oxides identified here in heterogeneous catalysis should be
188 considered when optimizing the size distribution, morphology, alloy composition and
189 core–shell structure of novel catalysts. Indeed, it was recently shown that the
190 electrochemical oxidation of Pt(111) could also proceed via a PtO-like surface oxide [2]
191 that is associated with a significant activation barrier for oxide reduction and that could,
192 in turn, be responsible for the overpotential of Pt-promoted ORR. This result accords
193 with the observation that the square-planar surface oxide reacts much less readily with
194 hydrogen than does chemisorbed oxygen [see Fig. 3(a)]: understanding oxide-related
195 degradation processes could therefore be critical for obtaining efficient and robust
196 catalysts for fuel-cell applications [2,38].

197 This work is supported by the Department of Energy, Office of Basic Energy
198 Sciences, Division of Materials Sciences and Engineering, under contract DE-AC02-
199 76SF00515, and by the Swedish National Research Council. This research was partly
200 carried out at the Advanced Light Source, an Office of Science User Facility operated for
201 the U.S. Department of Energy Office of Science by Lawrence Berkeley National
202 Laboratory. The DFT calculations were performed on resources provided by the Swedish
203 National Infrastructure for Computing (SNIC) at Center for Scientific and Technical
204 computing LUNARC.

205 *nilsson@slac.stanford.edu

206

207 See Supplemental Material at [*URL to be inserted*] for additional details regarding the
208 experimental setup and for a description of complementary XAS simulations performed
209 using the FEFF8.4 code.

210

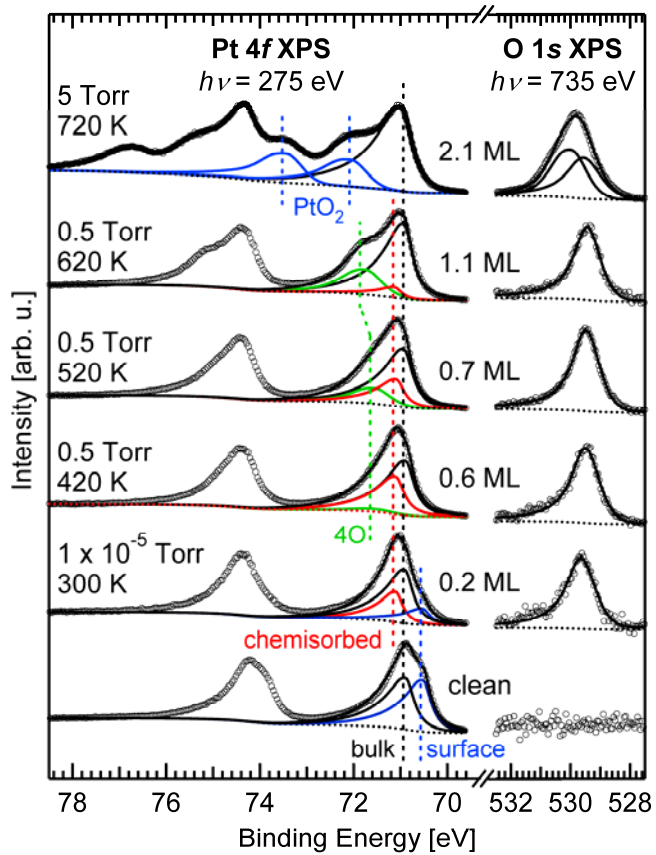
211 REFERENCES

- 212 [1] E. Lundgren *et al.*, J. Phys.: Condens. Matter **18**, R481 (2006).
- 213 [2] D. Friebe *et al.*, Phys. Chem. Chem. Phys. **13**, 262 (2011).
- 214 [3] M. D. Ackermann *et al.*, Phys. Rev. Lett. **95**, 255505 (2005).
- 215 [4] J. G. Wang *et al.*, Phys. Rev. Lett. **95**, 256102 (2005).
- 216 [5] A. L. Gerrard and J. F. Weaver, J. Chem. Phys. **123**, 224703 (2005).
- 217 [6] S. Günther *et al.*, J. Phys. Chem. C **112**, 15382 (2008).
- 218 [7] N. Seriani and F. Mittendorfer, J. Phys.: Condens. Matter **20**, 184023 (2008).
- 219 [8] C. Puglia *et al.*, Surf. Sci. **342**, 119 (1995).
- 220 [9] D. J. Miller *et al.*, J. Chem. Phys. **133**, 224701 (2010).
- 221 [10] S. P. Devarajan, J. A. Hinojosa Jr., and J. F. Weaver, Surf. Sci. **602**, 3116 (2008).
- 222 [11] R. Getman *et al.*, Phys. Rev. Lett. **102**, 076101 (2009).
- 223 [12] D. H. Parker, M. E. Bartram, and B. E. Koel, Surf. Sci. **217**, 489 (1989).
- 224 [13] C. R. Parkinson, M. Walker, and C. F. McConville, Surf. Sci. **545**, 19 (2003).
- 225 [14] J. F. Weaver, J. J. Chen, and A. L. Gerrard, Surf. Sci. **592**, 83 (2005).
- 226 [15] Y. S. Kim *et al.*, J. Chem. Phys. **133**, 034501 (2010).
- 227 [16] C. Ellinger *et al.*, J. Phys.: Condens. Matter **20**, 184013 (2008).

- 228 [17] D. F. Ogletree *et al.*, Rev. Sci. Instrum. **73**, 3872 (2002).
- 229 [18] Chemisorbed (oxide) slabs comprise four (five) atomic layers of Pt(111), two of
230 them fully relaxed, separated by 14 Å (15 Å) of vacuum and supporting O on one side,
231 see Ref. [9]. ($\sqrt{3} \times 2$) surface cells were used for all slabs except the oxide stripe, for
232 which a ($2\sqrt{3} \times 4$) cell was used. For α -PtO₂/Pt(111), we assumed coincidence between
233 ($\sqrt{3} \times \sqrt{3}$) $R30^\circ$ and (2×2) cells of the α -PtO₂(0001) trilayer and Pt(111), respectively.
234 This structure was optimized using computed spectra rather than the total energy, since
235 the neglect of van der Waals forces causes uncertainty in the vertical displacement, d_z , of
236 the Pt atoms in the trilayer from the topmost substrate layer. Varying d_z from 2.9 to 4.1 Å
237 while keeping Pt–O distances within the trilayer fixed yielded an optimal d_z of 3.5 Å.
- 238 [19] J. P. Perdew, K. Burke, and M. Ernzerhof, Phys. Rev. Lett. **77**, 3865 (1996).
- 239 [20] J. Enkovaara *et al.*, J. Phys.: Condens. Matter **22**, 253202 (2010).
- 240 [21] J. J. Mortensen, L. B. Hansen, and K. W. Jacobsen, Phys. Rev. B **71**, 035109
241 (2005).
- 242 [22] P. E. Blöchl, Phys. Rev. B **50**, 17953 (1994).
- 243 [23] PAW setups containing a half core-hole at the excited O were employed. The
244 XAS cross-section was obtained using the Haydock recursion scheme [R. Haydock *et al.*,
245 J. Phys. C: Solid State Phys. **5**, 2845-2858 (1972)] with 2000 Lanczos vectors to avoid
246 explicitly constructing the unoccupied states. The periodic boundary conditions
247 necessitated large supercells ($15 \times 15 \times 30 \text{ \AA}^3$) to eliminate core-hole interactions
248 between adjacent cells.
- 249 [24] L. Triguero, L. G. M. Pettersson, and H. Ågren, Phys. Rev. B **58**, 8097 (1998).
- 250 [25] M. P. Ljungberg, J. J. Mortensen, and L. G. M. Pettersson, J. Electron Spectrosc.,
251 in press, doi:10.1016/j.elspec.2011.05.004.

- 252 [26] The high-binding-energy tail of the O 1s feature arises from shake-up excitations
253 rather than from OH and H₂O species, which desorb from metallic Pt well below
254 300 K [8,30].
- 255 [27] R. B. Getman, Y. Xu, and W. F. Schneider, *J. Phys. Chem. C* **112**, 9559 (2008).
- 256 [28] J. M. Hawkins, J. F. Weaver, and A. Asthagiri, *Phys. Rev. B* **79**, 125434 (2009).
- 257 [29] M. Peuckert and H. P. Bonzel, *Surf. Sci.* **145**, 239 (1984).
- 258 [30] T. Schiros *et al.*, *J. Phys. Chem. C* **111**, 15003 (2007).
- 259 [31] J. Klikovits *et al.*, *J. Phys. Chem. B* **110**, 9966 (2006).
- 260 [32] S. A. Krasnikov *et al.*, *Nanotechnology* **21**, 335301 (2010).
- 261 [33] E. Lundgren *et al.*, *Phys. Rev. Lett.* **88**, (2002).
- 262 [34] W. X. Li *et al.*, *Phys. Rev. Lett.* **93**, 146104 (2004).
- 263 [35] S. Helveg *et al.*, *Surf. Sci.* **430**, L533–L539 (1999).
- 264 [36] J. Gustafson *et al.*, *Phys. Rev. Lett.* **92**, 126102 (2004).
- 265 [37] Y. B. He *et al.*, *J. Phys. Chem. C* **112**, 11946-11953 (2011).
- 266 [38] D. Friebel *et al.*, *Angew. Chem. Int. Ed.*, in press, doi:10.1002/anie.201101620.
- 267

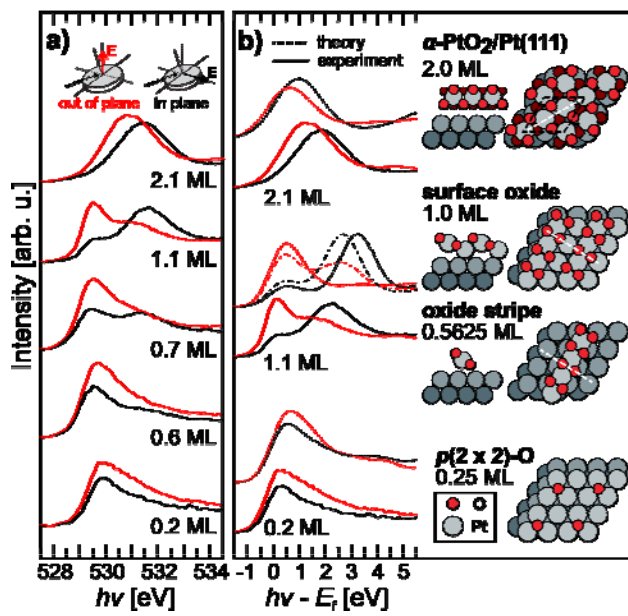
268 FIGURE 1



269

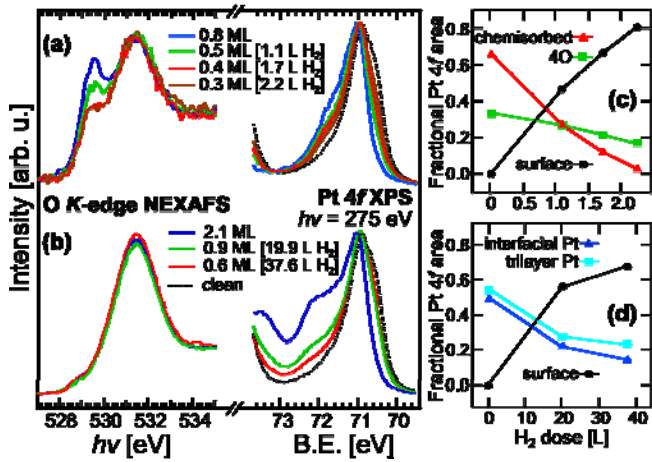
270

271 FIGURE 2



272

273 FIGURE 3



274

275 FIGURE CAPTIONS

276 FIG. 1 (color online). Pt 4*f* (left) and O 1*s* (right) XPS spectra for O/Pt(111),
277 deconvoluted using asymmetric Voigt and Gaussian-broadened Doniach-Šunjić
278 functions, respectively; a Shirley-type background (dashed line) was removed from all
279 spectra. Excepting $\theta = 2.1$ ML, which was prepared at [5 Torr, 720 K] but whose
280 spectrum was acquired at [0.5 Torr, 620 K], the same [$P(\text{O}_2)$, T] conditions were
281 employed for sample preparation and spectral acquisition.

282

283 FIG. 2 (color online). Experimental O *K*-edge XAS spectra (solid lines) are shown in (a)
284 and compared in (b) against simulations (dashed) of the adjacent model structures. Side
285 views of the model structures are cross sections along the dashed lines; the dashed
286 rhombus denotes a (2×2) supercell of the Pt(111) substrate. Results for the 1.0 ML
287 surface oxide and isolated oxide chain are shown using dashed and dashed-dotted lines,
288 respectively. Simulations were obtained by convoluting the GPAW output with a Gaussian
289 of 0.45 eV full-width at half-maximum (fwhm), except for α -PtO₂/Pt(111), for which
290 0.7 eV was used; these widths were determined from the fwhm of the associated O 1*s*
291 XPS peaks. Experimental spectra reflect removal of background signal from the Pt
292 substrate and were placed on a B.E. scale in (b) by subtracting the O 1*s* XPS B.E. All
293 spectra are area normalized ~ 30 eV above threshold.

294

295 FIG. 3 (color online). In-plane O *K*-edge XAS spectra (left) and Pt 4*f*_{7/2} XPS spectra
296 (right) obtained after H₂ treatment (2×10^{-8} Torr H₂ at 300 K) of Pt(111) oxidized at (a)
297 0.5 Torr O₂ and 570 K ($\theta = 0.8$ ML) and (b) 5 Torr O₂ and 720 K ($\theta = 2.1$ ML). XAS
298 spectra are area normalized ~ 30 eV above threshold. (c) and (d) show the fraction of the
299 total Pt 4*f* peak area associated with each oxygen phase as obtained by deconvoluting the
300 Pt 4*f* XPS spectra in (a) and (b), respectively.